Supporting Information

Realizing an Anolyte Utilization Rate of 99% in Low-cost Zinc-based Flow Batteries by Rejuvenating Dead Zinc

Shengnan Wang[1], Tianyu Li[2], Chenguang Yuan[2], Jiaxiong Zhu[1], Pei Li[1], Shaoce Zhang[1], Zhiquan Wei[1], Yiqiao Wang[1], Xianfeng Li[2], Chunyi Zhi*[1]*

[1]Department of Materials Science and Engineering, City University of Hong Kong, 83 Tat Chee Avenue, Kowloon, Hong Kong 999077, China

[2]Division of Energy Storage, Dalian Institute of Chemical Physics, Chinese Academy of Sciences, 457 Zhongshan Road, Dalian 116023, China

*Corresponding author.

E-mail: lixianfeng@dicp.ac.cn (X. Li); cy.zhi@cityu.edu.hk (C. Zhi)

Experimental section

Materials: Zinc oxide, potassium hydroxide, sodium hydroxide and sodium Hexacyanoferrate (II) were purchased from Aladdin (China). Bismuth oxide (Bi_2O_3) was purchased from Xindun-Alloy Co., Ltd. (China). Carbon felt (CF) was purchased from Liaoyang J-Carbon Materials Co., Ltd. (China) and used as received. All electrolytes were prepared with deionized water.

Materials Characterization: The microstructure and elemental distribution of Zn, Bi and Bi_2O_3 deposits were characterized by field emission scanning electron microscope (SEM, JEOL-7001F) equipped with an energy-dispersive X-ray spectroscopy (EDS). The X-ray diffraction (XRD) patterns of deposits were tested using an X-ray diffractometer (Rigaku SmartLab 9kW). X-ray photoelectron spectroscopy (XPS) spectra were collected on the Thermo Scientific K-Alpha equipment. The contents of Zn and Bi elements in the electrolyte were analyzed by inductively coupled plasma mass spectrometry (Agilent 720ES).

Zn//Bi$_2$O$_3$ Coin Battery: For the cathode, Bi_2O_3 powder, active carbon and PVDF binder were mixed in N-Methyl-2-pyrrolidone (NMP) solvent with a mass ratio of 8:1:1.[1] The mixture was grounded in a mortar for at least 30 mins to form a paste and then coated the paste onto a piece of carbon cloth paper. The cathode electrode was finally obtained after drying at 60 °C. The effective mass loading of the Bi_2O_3 cathode was consistent. Zn//Bi_2O_3 batteries were assembled in CR2032-type coin cells in an air atmosphere, ~75 μL electrolyte, using zinc foil (50 μm) as anode and glass fiber filter (Whatman, GF/C) as the separator. The battery performance was performed by a LAND battery charge/discharge system of CT3001A series (China).

Full Battery Performance: The alkaline zinc-iron flow battery (AZIFB) was assembled by sandwiching a membrane between two CF electrodes clamped by two graphite plates. The active area of the electrode is 2×2 cm^2. The polybenzimidazole (PBI) membrane was used to separate the catholyte and anolyte.[2] The anolyte contains 0.3 mol L^{-1} $Zn(OH)_4^{2-}$ and 3.2 mol L^{-1} OH^- or 0.5 mol L^{-1} $Zn(OH)_4^{2-}$ and 3 mol L^{-1}

OH^-. The catholyte contains 0.6 mol L^{-1} $Fe(CN)_6^{4-}$ and 3 mol L^{-1} OH^-. The different concentration electrolytes were used to flow pass the batteries. The batteries were operated at a constant current density and the charge process was controlled by the capacity of anolyte. According to the volume of added anolyte, the capacity released when the anolyte utilization rate (AUR) is 100% can be calculated. Considering the influence of side reactions, etc., the charging process was controlled by a capacity of 99% anolyte utilization rate or a protecting cutoff voltage. The discharge process was ended with a cutoff voltage of 0.1 V. The utilization rate of catholyte is 50%. For the flow batteries with Bi_2O_3, an excess of Bi_2O_3 was added to the anolyte tank, with the initial addition amount being 1 g. To optimize dead zinc recovery, the added Bi_2O_3 was spread flat on the bottom of the tank. When the taupe Bi product is observed spreading over the yellow Bi_2O_3, the mixture of Bi and Bi_2O_3 should be stirred to ensure that the dead zinc is in contact with the Bi_2O_3. During long-cycle battery testing, when a significant amount of taupe product is observed at the bottom of the tank, 1 g of fresh Bi_2O_3 should be added to the tank to maintain a stable supply of Bi_2O_3. All the battery performance tests were conducted by CT3001A, LAND Battery Testing System.

Zn//CF flow battery: Similar to full battery assembling, the Zn//CF flow cell was assembled by using Zn plate (2 cm×2 cm×0.05 cm) attached CF (2 cm×2 cm×0.42 cm) as cathode, CF (2 cm×2 cm×0.5 cm) as anode. The electrolytes flowing past the positive and negative electrodes of the battery were identical, containing 0.3 mol L^{-1} $Zn(OH)_4^{2-}$ and 3.2 mol L^{-1} OH^-. And the PBI membrane was used to separate the catholyte and anolyte. The test was carried out by plating a given amount of Zn metal onto the CF substrate, followed by stripping Zn metal from the CF substrate with a cut-off voltage.

Ab-initio **Calculations:** The absorption energy (E_a) was carried out by Vienna *Ab-initio* Simulation Package (VASP)[3], within the framework of density functional theory (DFT). Electronic exchange and correlation energies were treated at the level of generalized gradient approximation (GGA)[4] with the Perdew, Burke, and Ernzerhof (PBE) functional.[5] The core electrons were treated with the projector-augmented wave (PAW)[6] method. Vander Waals interaction was taken into account at DFT-D3[7, 8] with

Becke-Jonson (BJ)[9] damping level. The plane wave cutoff was set to 500 eV. A 15 Å-width vacuum was added along the vertical direction normal to the surfaces. The Brillouin zone integration was carried out with 3×3×1 Gamma point. The convergence thresholds for energy were set as 10^{-5} eV during ion relaxation, and the convergence thresholds for force were set as 0.02 eV Å^{-1}. The absorption energy can be obtained by the following equation,

$$E_a = E_{\text{Zn-substrate}} - E_{\text{Zn}} - E_{\text{substrate}}$$

where $E_{\text{Zn-substrate}}$, E_{Zn}, and $E_{\text{substrate}}$ represent the energies of the Zn adsorbed metal surface, Zn atom, and the clean metal surface, respectively.

Comsol **Multiphysics Simulation:** A two-dimensional stationary model was constructed to simulate the ion distribution for AZIFBs with and without Bi_2O_3. The model was built by employing Darcy's Law and the tertiary current distribution physical field and solved by the commercial package COMSOL Multiphysics®. The simulation considered the coupling effect of electric, concentration, and velocity fields. The computational domain included positive and negative electrodes and membranes. The area of the electrode is 2×2 cm^2, the thickness is 5 mm, and the membrane thickness is 900 μm. The positive and negative electrodes were both porous CF with a porosity of 90%. The electrode boundary condition was set to velocity inlet, and the inflow velocity in the normal direction was set to 2 mm/s. The electrode outlet boundary condition was set to pressure outlet and set to atmospheric pressure. The diffusion coefficient of different ions is shown in Supplementary Table 3. The solver was PARDISO, and the relative error tolerance was set to 0.001. The simulation employs the galvanostatic method with a current density of 80 mA cm^{-2}, which is consistent with the experimental conditions. The $Zn(OH)_4^{2-}$ ion concentrations at the beginning of the 100th charge were calculated to be 0.3 mol L^{-1} and 0.147 mol L^{-1} for the batteries with and without Bi_2O_3, respectively, based on the charge capacity values in Figure 4a. The initial concentrations of $Fe(CN)_6^{4-}$ in AZIFBs were all 0.6 mol L^{-1}. The electronic conductivity is $0.8×10^6$ S/m and $1.5×10^3$ S/m for the cases with and without Bi_2O_3, respectively.[10]
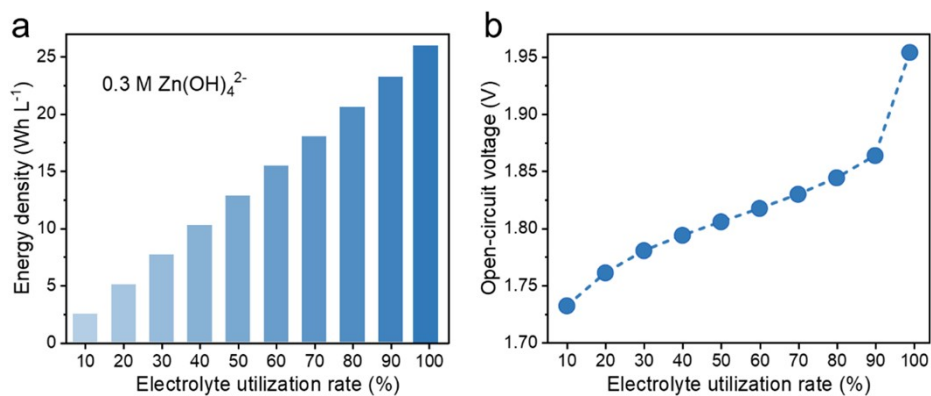
Supplementary Figures

Figure S1. (a) Energy density and (b) the corresponding open-circuit voltage of AZIFB at a $Zn(OH)_4^{2-}$ concentration of 0.3 mol L^{-1} at different electrolyte utilization rates.

As the electrolyte utilization rates increases from 10 to approximately 100%, the energy density and open-circuit voltage (OCV) increase monotonically. High OCV in combination with operating current density is expected to afford the battery with a high power density.
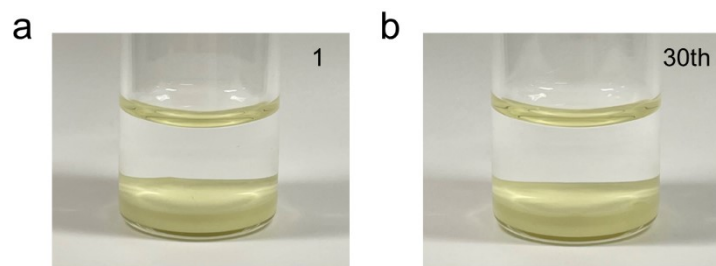
Figure S2. Digital photograph of Bi_2O_3 powder before and after being immersed in the alkaline electrolyte for 30 days.
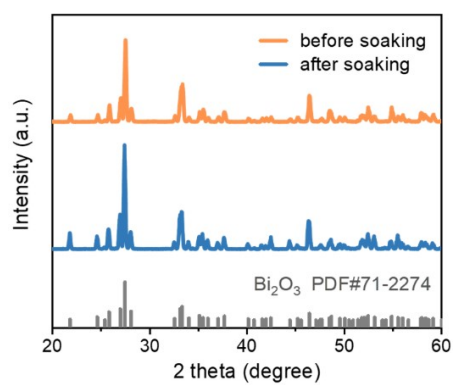
Figure S3. XRD pattern of Bi_2O_3 before and after soaking in electrolyte for 30 days.
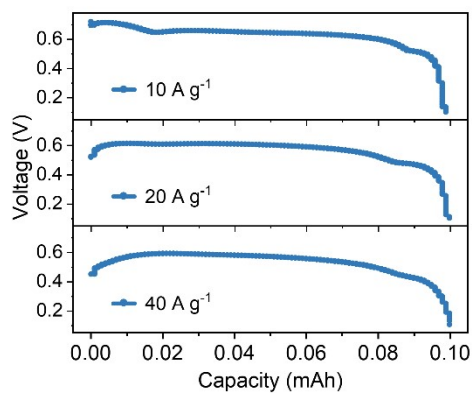
Figure S4. Galvanostatic discharge profiles at 10, 20, and 40 A g^{-1} in a Zn//Bi$_2$O$_3$ coin battery.
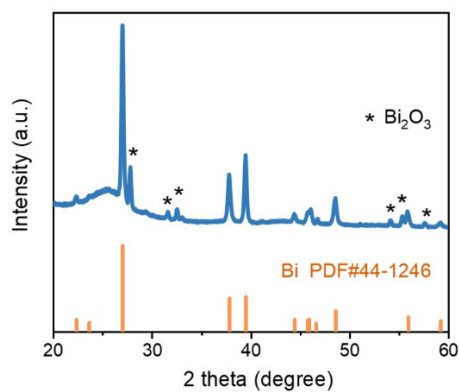
Figure S5. XRD pattern of the cathode of Zn//Bi$_2$O$_3$ battery after discharge.
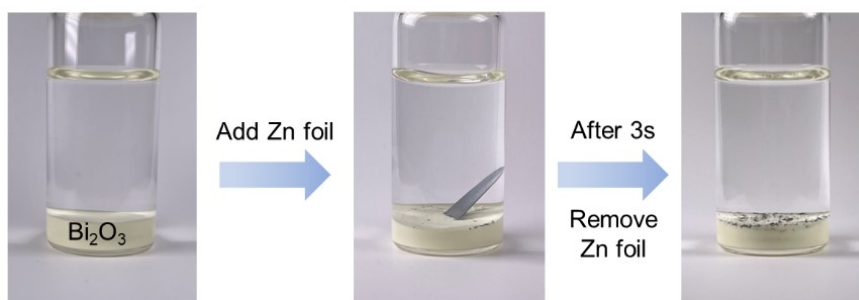
Figure S6. Digital photograph of Bi_2O_3 in the electrolyte before and after adding zinc foil.
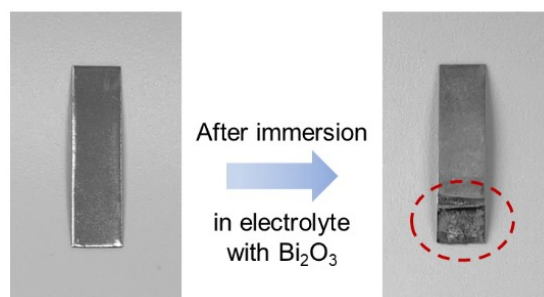
Figure S7. Digital photograph of zinc foil before and after touching Bi_2O_3 in the electrolyte.
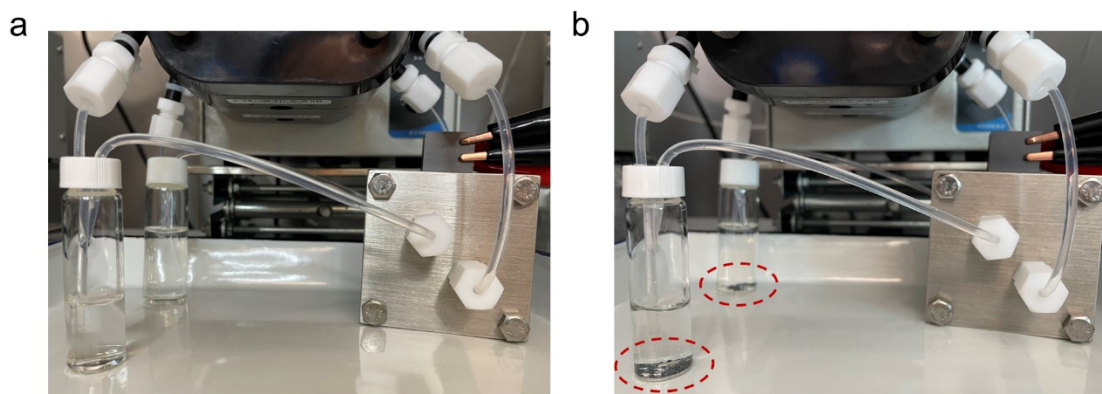
Figure S8. Digital photographs of the Zn//CF flow cell without Bi_2O_3 in operation during the (a) 1st and (b) 120th charge at 80 mA cm^{-2}. The utilization rates of anolyte and catholyte were 99% and ~50%, respectively. These unevenly deposited zinc dendrites can lose contact with the electrode and turn into dead zinc. The zinc that falls off from the CF electrode flows with the electrolyte to the storage tank. Since the density of zinc (7.14 g·cm^{-3}) is much greater than the density of the electrolyte (~1.16 g·cm^{-3} for 0.3 mol L^{-1} $Zn(OH)_4^{2-}$ and 3.2 mol L^{-1} OH^-), dead zinc will settle at the bottom of the tank and completely lose the chance to contact the electrode.

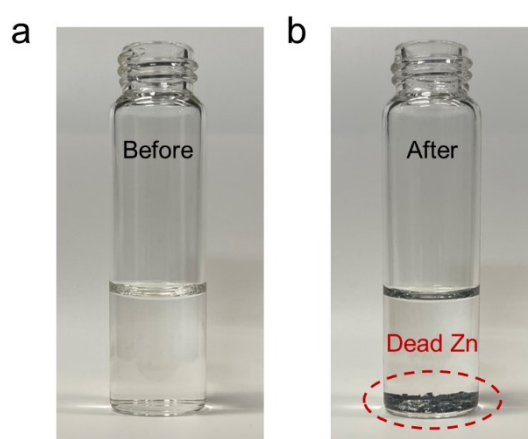
Figure S9. Digital photographs of the anolyte at an anodic tank before and after 120 cycles at 80 mA cm^{-2} under an areal capacity of 23.8 mAh cm^{-2}.
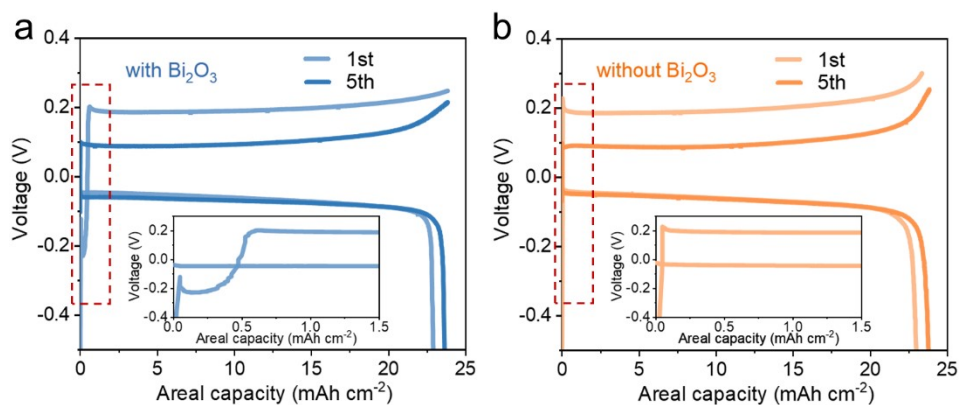
Figure S10. Galvanostatic charging–discharging profiles at the 1st and 5th cycles of Zn//CF flow cells (a) with and (b) without Bi_2O_3 at 80 mA cm^{-2}. The inset shows corresponding detailed voltage profiles at the 1st cycle of Zn//CF flow cell with and without Bi_2O_3 marked by red rectangles.
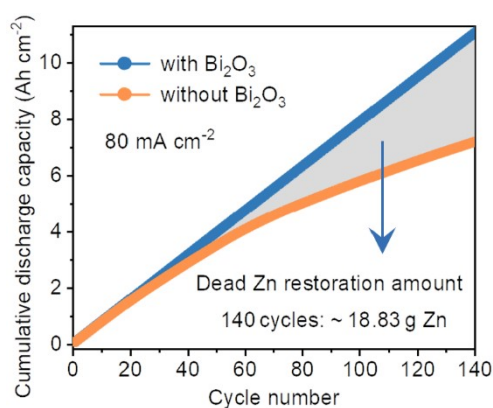

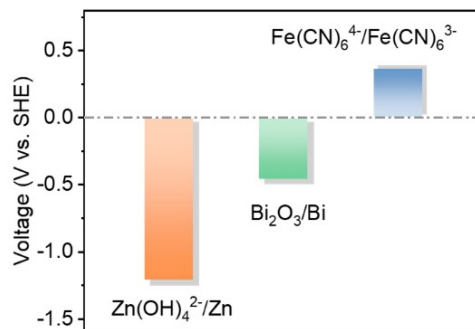Figure S11. Regeneration amount of dead zinc in Zn//CF flow cell with Bi_2O_3 during battery operation.

Figure S12. Various potential differences of $Zn(OH)_4^{2-}/Zn$, Bi_2O_3/Bi and $Fe(CN)_6^{4-}/Fe(CN)_6^{3-}$ redox couples.
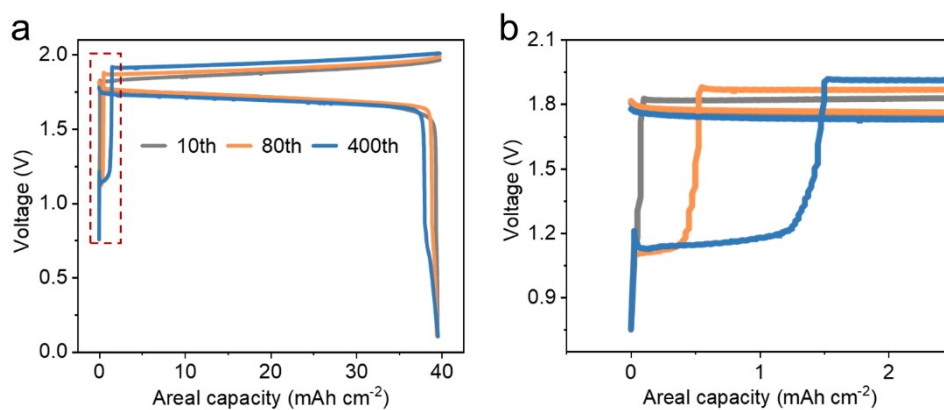

Figure S13. (a) Galvanostatic charging–discharging profiles at the 10th, 80th, and 400th cycles of an AZIFB with Bi_2O_3 and (b) the corresponding detailed voltage profiles marked by red rectangles.
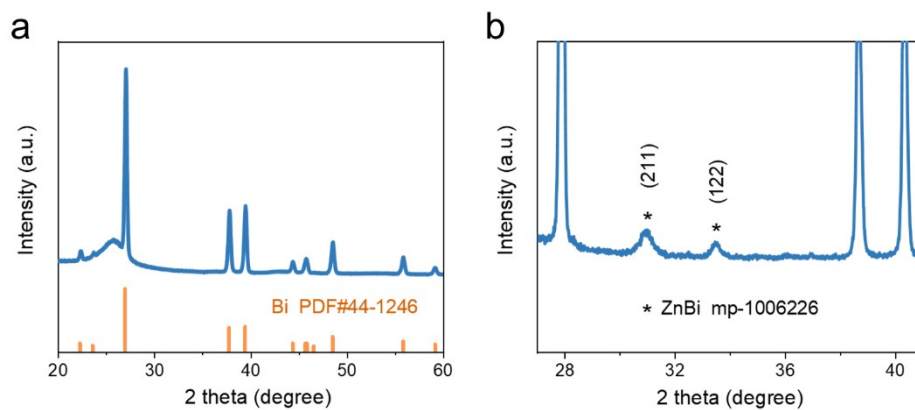
Figure S14. (a) XRD pattern of the anodic carbon felt charged to 1.6 V for the 75th cycle of AZIFB with Bi_2O_3. (b) Partially magnified XRD pattern of the anodic carbon felt.
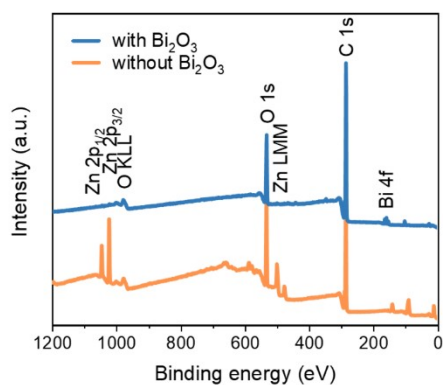

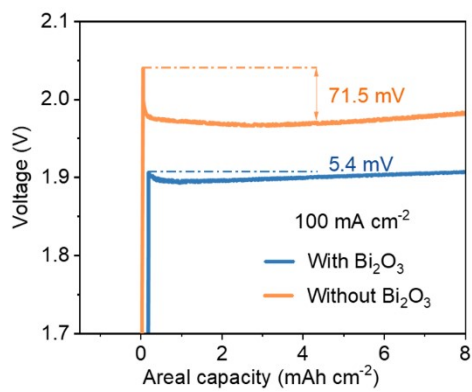Figure S15. XPS spectra of the charged anodic carbon felt taken from AZIFB with and without Bi_2O_3.

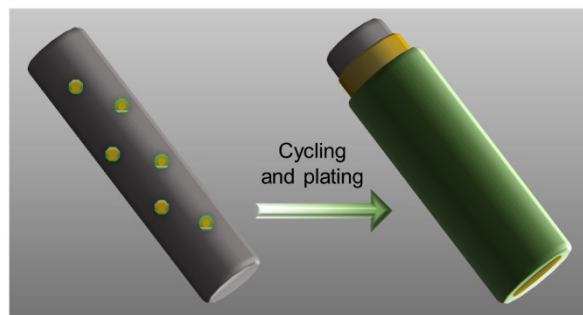Figure S16. Polarization curves of Zn deposition of AZIFBs with and without Bi_2O_3 at 100 mA cm^{-2}.

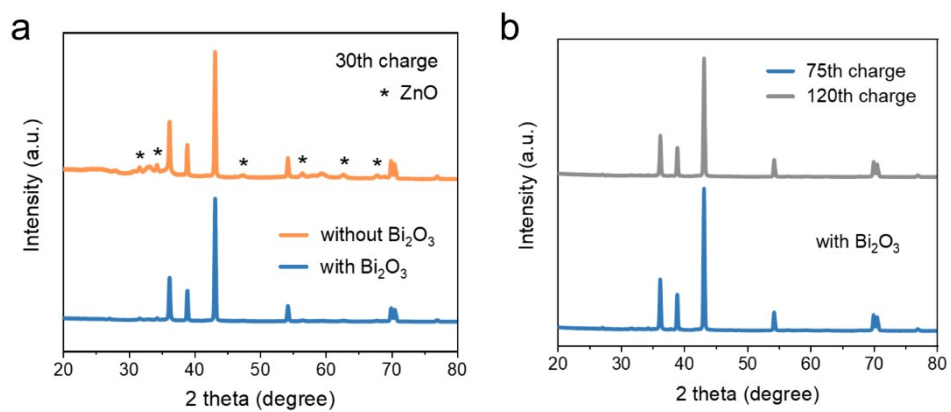Figure S17. A schematic illustration of Zn plating on Bi@Zn interface.

Figure S18. (a) XRD patterns of the Zn deposit at the 30th end of charging of the AZIFBs with and without Bi_2O_3. (b) XRD patterns of the Zn deposit at the 75th and 120th end of charging for the AZIFBs with Bi_2O_3.
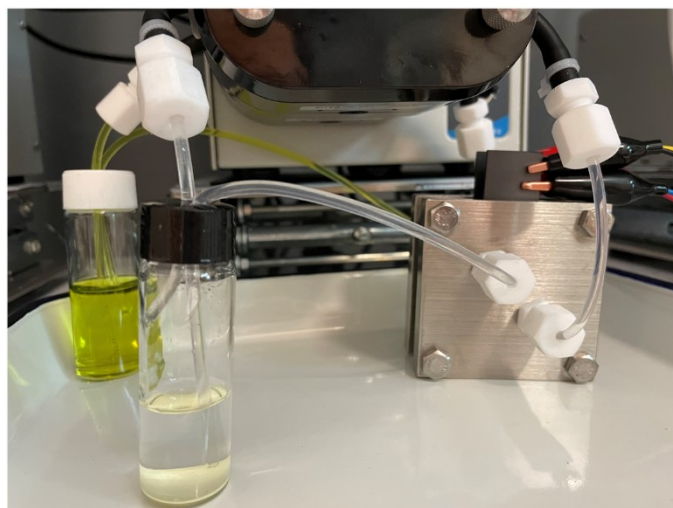

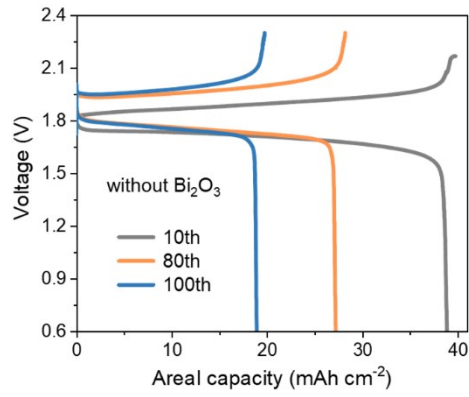Figure S19. Digital photograph of AZIFB with Bi_2O_3.

Figure S20. Voltage profiles at the 10th, 80th, and 100th cycles of AZIFB without Bi_2O_3 at 80 mA cm^{-2}.
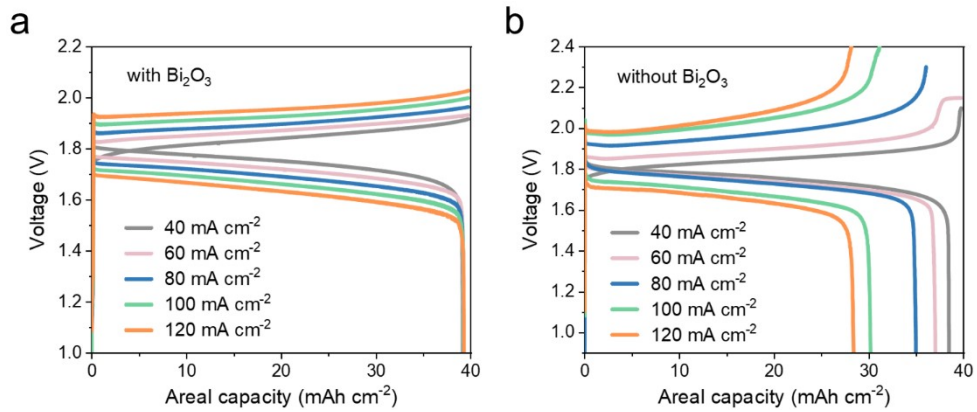
Figure S21. Voltage profiles of AZIFBs (a) with and (b) without Bi_2O_3 at current densities ranging from 40 to 120 mA cm^{-2}.
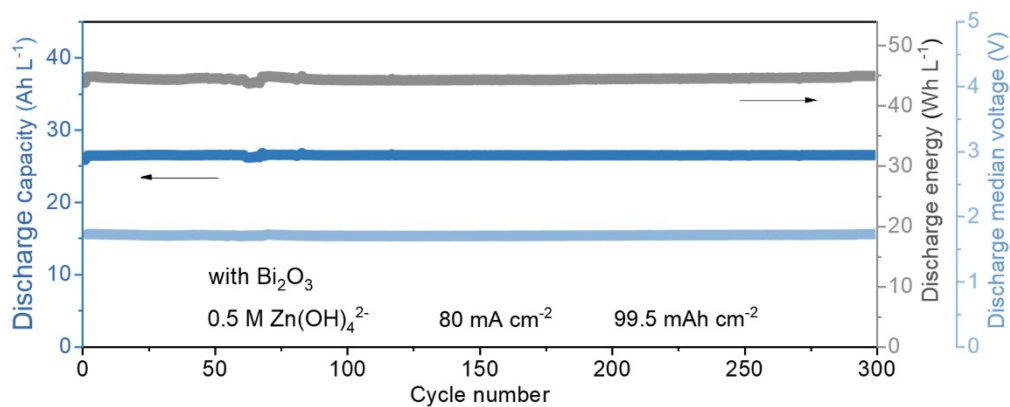
Figure S22. Discharge capacity, discharge energy and discharge median voltage of an AZIFB with Bi_2O_3 at a $Zn(OH)_4^{2-}$ concentration of 0.5 mol L^{-1} at 80 mA cm^{-2}.
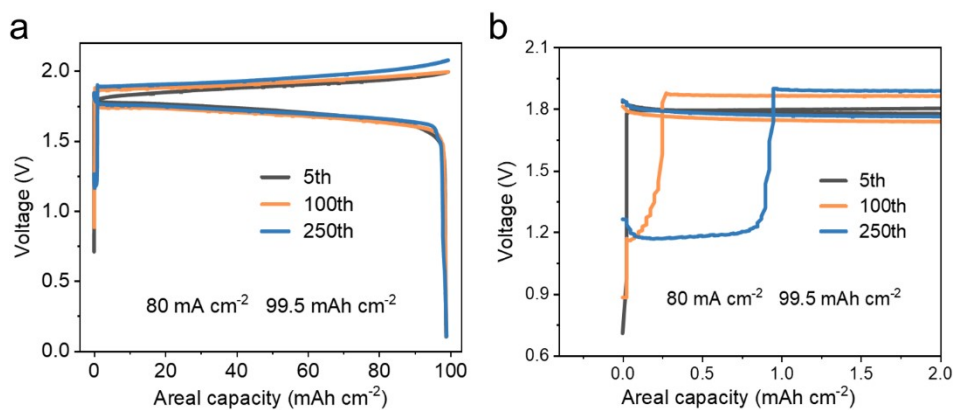
Figure S23. (a) Voltage profiles at the 5th, 100th, and 250th cycles of an AZIFB with Bi_2O_3 at a $Zn(OH)_4^{2-}$ concentration of 0.5 mol L^{-1}. (b) Detailed voltage profiles at the beginning of charging.

Figure S24. Cycling performance of AZIFBs with and without Bi_2O_3 at 160 mA cm^{-2}.

Figure S25. Long-term performance of an AZIFB without Bi_2O_3 at a $Zn(OH)_4^{2-}$ concentration of 0.5 mol L^{-1} at 80 mA cm^{-2}.
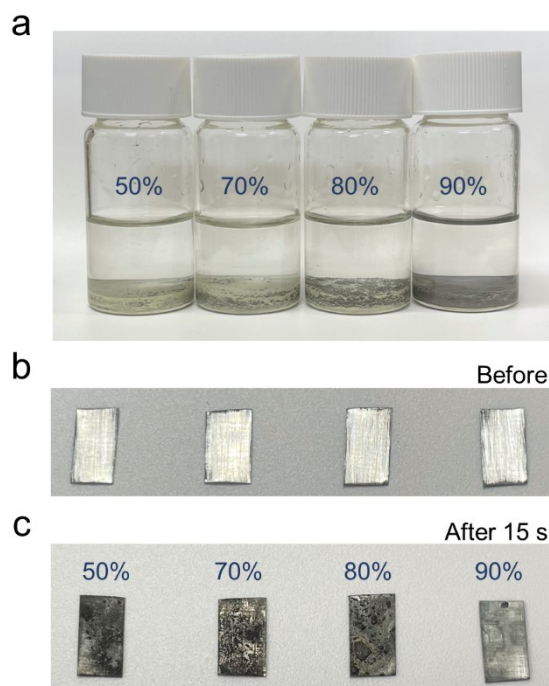
Figure S26. (a) Digital photograph of the mixture of Bi_2O_3 and Bi immersed in the electrolyte when Bi_2O_3 was converted to Bi at 50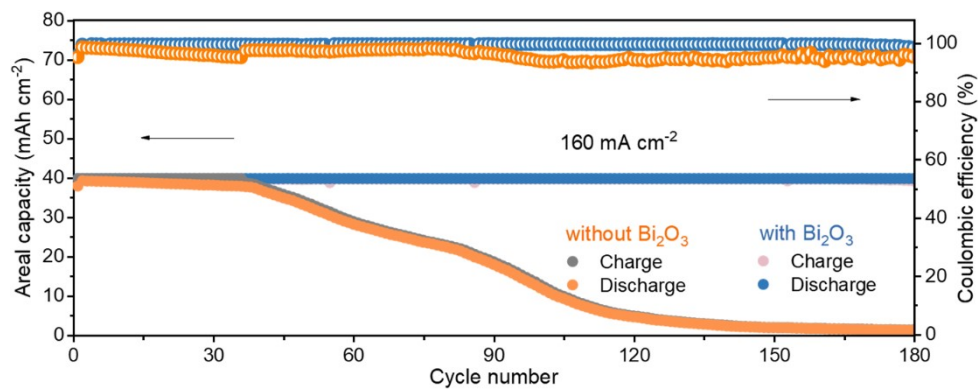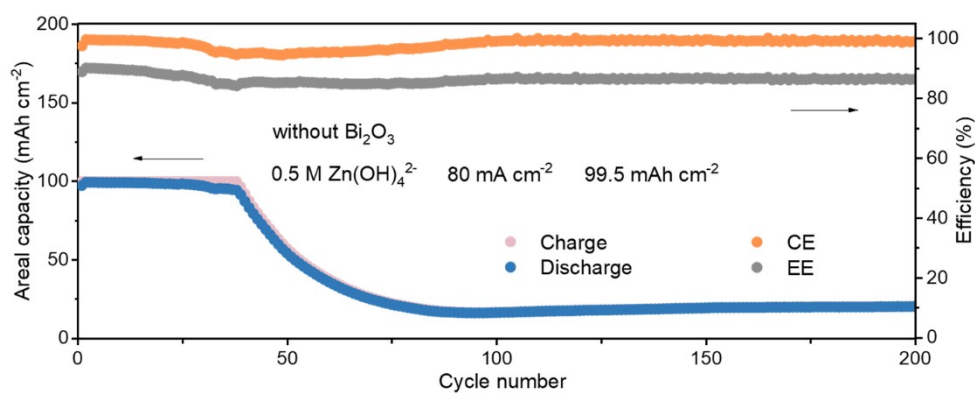%, 70%, 80%, and 90%, respectively. The mixture was obtained by adding different amounts of Bi_2O_3 and Bi to the electrolyte and stirring, assuming that the initial amount of Bi_2O_3 added is 5g. Digital photographs of zinc foil (b) before and (c) after being placed in the above mixture, and taken out after 15 s.

When 50%, 70% and 80% of the Bi_2O_3 were converted to Bi, there is a noticeable taupe Bi product formed on the surface of the zinc foil upon immersion in the above-mentioned mixture, consistent with the phenomenon when fresh Bi_2O_3 is used (Figure S6). When the conversion rate of Bi_2O_3 rises to 90%, the taupe product on the surface of the zinc foil decreases, indicating that the insufficient Bi_2O_3 content affects the reaction rate with zinc. Therefore, during long-term battery operation, Bi_2O_3 can be used at a conversion rate of approximately 80%, which still has a good effect on regenerating dead zinc.
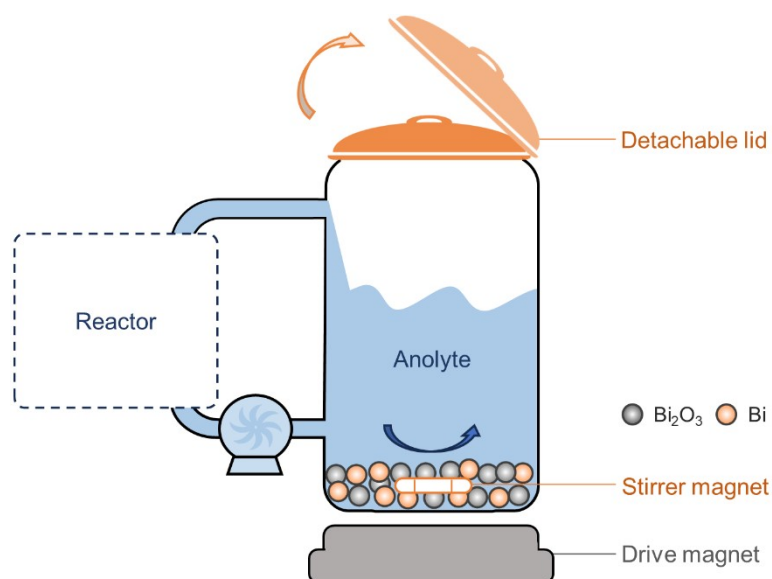
Figure S27. Schematic diagram of a storage tank with stirring and Bi_2O_3 addition functions.

Supplementary Tab. 1. The bulk price of chemicals.[2, 11]

Chemical	Molecular weight (g mol^{-1})	Price (US$ kg^{-1})
ZnO	81.39	1.3
NaOH	40.00	0.34
NaCl	58.44	0.13 [a]
Bi_2O_3	465.96	10 [b]
Bi	208.98	35 [c]

[a] The cost information is shown in Ref. 17.
[b] The cost information is shown in Ref. 18.
[c] The cost information is shown in Ref. 19.

Supplementary Tab. 2. The anolyte cost for AZIFBs.

Anolyte composition	Anolyte utilization	Energy density	Anolyte cost (US$ KWh^{-1})	Source
0.5M $Zn(OH)_4^{2-}$ +4M NaOH	53.1	40.00	5.70	2
0.4M $Na_2Zn(OH)_4$ +3M NaOH	74.6	30.71	4.10	12

0.4M $Zn(OH)_4^{2-}$ +3M NaOH	70.8	26.78	4.96	[13]
0.4M $Zn(OH)_4^{2-}$ +3M OH^-	70.0	23.87	5.63	[14]
0.5M $Zn(OH)_4^{2-}$ +4M NaOH	67.4	31.45	5.07	[15]
0.3M $Na_2Zn(OH)_4$ +2.4M NaOH+0.5M NaCl	70.0	25.00	4.36	[16]
0.5M $Zn(OH)_4^{2-}$ +3M OH^-	99.0	44.75	2.42	
			Cost of Bi_2O_3: 5.28 Value of recycled Bi: 16.57 Income of Bi: 11.29	In this work

Supplementary Tab. 3. The diffusion coefficient of different ions.[20]

Ions	Value (cm^2/s)
$Zn(OH)_4^{2-}$	1.2×10^{-6}
OH^-	5.3×10^{-5}
K^+	1.9×10^{-5}
$Fe(CN)_6^{4-}$	7.8×10^{-6}
$Fe(CN)_6^{3-}$	8.2×10^{-6}

Reference

1.   Wang D, *et al.* A zinc battery with ultra-flat discharge plateau through phase transition mechanism. *Nano Energy* **71**, 104583 (2020).

2.   Yuan Z, Duan Y, Liu T, Zhang H, Li X. Toward a Low-Cost Alkaline Zinc-Iron Flow Battery with a Polybenzimidazole Custom Membrane for Stationary Energy Storage. *iScience* **3**, 40-49 (2018).

3.   Kresse G, Furthmüller J. Efficient iterative schemes for ab initio total-energy calculations using a plane-wave basis set. *Phys. Rev. B* **54**, 11169-11186 (1996).

4.   Perdew JP, Burke K, Ernzerhof M. Generalized Gradient Approximation Made Simple. *Phys. Rev. Lett.* **77**, 3865-3868 (1996).

5.   Perdew JP, Ernzerhof M, Burke K. Rationale for mixing exact exchange with density functional approximations. *J. Chem. Phys.* **105**, 9982-9985 (1996).

6.   Blöchl PE. Projector augmented-wave method. *Phys. Rev. B* **50**, 17953-17979 (1994).

7.   Grimme S. Density functional theory with London dispersion corrections. *Wiley Interdisciplinary Reviews: Computational Molecular Science* **1**, 211-228 (2011).

8.   Grimme S. Accurate description of van der Waals complexes by density functional theory including empirical corrections. *J Comput Chem* **25**, 1463-1473 (2004).

9.   Johnson ER, Becke AD. A post-Hartree-Fock model of intermolecular interactions: Inclusion of higher-order corrections. *J. Chem. Phys.* **124**, 174104 (2006).

10.   Ma X, Zhang H, Xing F. A three-dimensional model for negative half cell of the vanadium redox flow battery. *Electrochim. Acta*, **58,** 238-246 (2011).

11.   Li Z, Lu Y-C. Polysulfide-based redox flow batteries with long life and low levelized cost enabled by charge-reinforced ion-selective membranes. *Nat. Energy* **6**, 517-528 (2021).

12.   Yuan Z, *et al.* Low-cost hydrocarbon membrane enables commercial-scale flow batteries for long-duration energy storage. *Joule* **6**, 884-905 (2022).

13.   Yuan Z, Liu X, Xu W, Duan Y, Zhang H, Li X. Negatively charged nanoporous membrane for a dendrite-free alkaline zinc-based flow battery with long cycle life. *Nat. Commun.* **9**, 3731 (2018).

14.   Hu J, *et al.* Layered double hydroxide membrane with high hydroxide conductivity and ion selectivity for energy storage device. *Nat. Commun.* **12**, 3409 (2021).

15.   Chen Z, *et al.* Mathematical modeling and numerical analysis of alkaline zinc-iron flow batteries for energy storage applications. *Chem. Eng. J.* **405**, 126684 (2021).

16.   Gong K, *et al.* A zinc–iron redox-flow battery under $100 per kW h of system capital cost. *Energy Environ. Sci.* **8**, 2941-2945 (2015).

17.   Sodium Chloride Industry Grade 99%. Available at https://www.alibaba.com (Accessed: 19th July 2023).

18.   Factory price Bismuth Oxide/Bismuth Trioxide powder. Available at https://www.alibaba.com (Accessed: 19th July 2023).

19.   Factory Sale Metal Bismuth Powder Price. Available at https://www.alibaba.com (Accessed: 19th July 2023).

20.   Wu J, Yuan C, Li T, Yuan Z, Zhang H, Li X. Dendrite-Free Zinc-Based Battery with High Areal Capacity via the Region-Induced Deposition Effect of Turing Membrane. *J. Am. Chem. Soc.* **143**, 13135-13144 (2021).